



Trans. Nonferrous Met. Soc. China 34(2024) 2020-2033

Transactions of Nonferrous Metals Society of China

www.tnmsc.cn



Effect of As and MgO addition on arsenic vitrification in copper smelting slag

Zhe-nan JIN^{1,2}, Bao-ren WANG^{1,2}, Hong-ying YANG^{1,2}, Qian-fei ZHAO^{1,2}, Yan FU^{1,2}

Key Laboratory for Ecological Metallurgy of Multi-metallic Mineral of Education Ministry,
 Northeastern University, Shenyang 110819, China;

 School of Metallurgy, Northeastern University, Shenyang 110819, China

Received 11 November 2022; accepted 18 July 2023

Abstract: The arsenic (As) vitrification in copper smelting slag derived from the FeO–SiO₂–Fe₂O₃–B₂O₃–CaO–Al₂O₃–(MgO) system was studied. The vitrification mechanism of As was systematically investigated by XRD, SEM, FTIR and XPS analysis. It is determined that As exhibits favorable compatibility with the iron-silicate slag. FTIR and XPS analysis indicates that As can partially substitute for silicon to form the Si–O—As structure, thereby enhancing the degree of polymerization of the melt. The [BO₃]³⁻ unit tends to decrease with the increase of the As content, while the opposite behavior is observed with the addition of MgO. Additionally, MgO increases the non-bridging oxygen (NBO) number of the melt. TCLP, SPLP and pH dependence tests show that the leaching toxicity of As increases with the increase of the As content but decreases with the addition of MgO. DSC analysis demonstrates that the incorporation of both As and MgO can improve the thermal stability of the As-containing glass.

Key words: vitrification; As; MgO; copper smelting slag; slag structure

1 Introduction

At present, 75% to 80% of the global mine copper production comes from pyrometallurgy of copper concentrate [1,2]. As arsenic is often associated with copper concentrate and extremely harmful to smelting process and environmental protection, the continuous growth of copper production poses a severe challenge to the reduction of pollutants in non-ferrous metal industry [3]. In the process of copper smelting, arsenic enters the wastewater, flue gas, slag or products in the form of sulfide, oxide, arsenate and arsenite, causing a series of problems in the subsequent processes of sulfuric acid, refining and electrolysis [4–6]. The traditional metallurgical process focuses on the recycling of valuable metals and puts the

management of arsenic pollution on the back burner. Consequently, harmless treatment of arsenic-containing materials is the fundamental way to solve the arsenic pollution in copper smelting enterprises.

To date, the research on the disposal of arsenic-containing materials mainly focuses on the chemical precipitation [7–9], stabilization/solidification treatment [10–12], and resource utilization [13,14]. These approaches are typically implemented through the hydrometallurgy and pyrometallurgy techniques. However, it has been demonstrated that these methods possess inherent limitations. For instance, the products generated often exhibit poor long-term stability [15], the utilization rate of arsenic residue is low, and controlling the production process proves challenging [16], resulting in the potential release

of arsenic into the environment. Vitrification, a enables technology that the immobilization of arsenic during the smelting process, has garnered increasing attention from researchers due to its ability to safely disposing arsenic contaminants in their source [17–19]. Vitrified products demonstrate favorable chemical stability and mechanical strength, making them suitable for applications as general landfill or construction materials. In a study by REDDY and FONT [20], thermodynamic modeling was employed to predict the impact of different slag compositions on arsenate capacity. The calculations revealed that the addition of CaO and MgO at 1250 °C can enhance the arsenic fixation capacity of the slag. In terms of specific experimental investigations, the GlassLock ProcessTM developed by Dundee Sustainable Technologies (DST), a Canadian company, has been utilized for vitrifying industrial arseniccontaining waste. By melting arsenic-bearing soot, silica, waste glass, and hematite at high temperatures, stable glass containing up to 20 wt.% As can be obtained [21-23]. ZHAO et al [24] conducted a study in which sodium arsenate was mixed with crushed glass and subjected to high-temperature results demonstrated The immobilization of arsenic in the SiO2-B2O3-Na2O-Al₂O₃ system remained above 99%. Furthermore, BHARGAVA et al [25] employed B₂O₃ to modify the properties of BaO-TiO₂-B₂O₃ glass, thus enhancing its ability to fix arsenic.

Although some studies have been conducted on the vitrification of arsenic in iron-silicate slag systems, the majority of these investigations have primarily focused on oxidizing slag systems characterized by high Fe₂O₃ content. Conversely, there has been a paucity of research on reducing slag systems containing high FeO contents. Nevertheless, it is worth noting that the prevailing copper smelting process typically entails relatively low Fe₂O₃ content in the slag to ensure optimal fluidity and smoothness during smelting operations. Furthermore, the capacity of iron olivine slag to accommodate arsenic remains unclear, necessitating a thorough examination. Additionally, the chemical stability of the resultant vitrification product necessitates further investigation. Another aspect that merits attention is the presence of minute quantities of MgO in the molten slag, as its impact arsenic vitrification has been scarcely documented. Consequently, a comprehensive study addressing the vitrification of arsenic in ironsilicate slag systems is imperative.

In this work, the effects of As (0-4 wt.%) and MgO (0-3 wt.%) contents on arsenic vitrification in the simulated copper smelting slag FeO-SiO₂-Fe₂O₃-B₂O₃-CaO-Al₂O₃-(MgO) system were investigated. Additionally, an analysis of actual industrial slag was conducted to facilitate meaningful comparison. The stability of arsenic was assessed using established methodologies such as the toxicity characteristic leaching procedure (TCLP, **USEPA** method 1311), synthetic precipitation leaching procedure (SPLP, USEPA method 1312), and pH dependency method (1313) [22,23]. In addition, the mechanism of arsenic vitrification was studied by XRD, SEM, FTIR, XPS method and differential scanning calorimetry (DSC). This work is devoted to the safe disposal of arsenic-containing hazardous waste in copper smelting industry, aiming to provide valuable insights for enterprises engaged in clean production and environmental protection endeavors.

2 Experimental

2.1 Sample preparation

The chemicals employed in the experiments, namely CaO, SiO₂, Fe₂O₃, B₂O₃, Al₂O₃, MgO, and iron powder, were of analytical purity. FeO was generated on-site at elevated temperatures by maintaining a molar ratio of 1.0 between iron powder and Fe₂O₃. To enhance arsenic stability at high temperatures and minimize its volatilization, calcium arsenate was utilized as the arsenic source in the samples. Calcium arsenate was synthesized in the laboratory and contained 29.1 wt.% As and 38.0 wt.% Ca, with its corresponding XRD pattern illustrated in Fig. S1(a) in Supporting Information. The detailed procedure for the preparation of calcium arsenate has been documented in our previous study [26]. Because calcium arsenate contributes calcium to the samples, different levels of CaO were incorporated to maintain a constant overall calcium quantity. The Fe/SiO₂ mass ratio, defined as the mass ratio of total Fe to SiO2 in the sample, was consistently set to 1.2:1 throughout the experiment. The predetermined chemical compositions of the simulated slag system (Slag 1 – Slag 7) are outlined in Table 1.

Table 1 Predetermined chemical compositions of glass samples

Sample ID	Fe/SiO ₂ mass ratio	Content/wt.%							
		FeO	SiO_2	Fe_2O_3	B_2O_3	Al_2O_3	CaO	MgO	As
Slag 1	1.2:1	44.96	32.04	5	5	3	10	0	0
Slag 2	1.2:1	44.51	31.72	4.95	4.95	2.97	9.9	0	1
Slag 3	1.2:1	44.06	31.40	4.9	4.9	2.94	9.8	0	2
Slag 4	1.2:1	43.61	31.08	4.85	4.85	2.91	9.7	0	3
Slag 5	1.2:1	43.16	30.76	4.80	4.80	2.88	9.6	0	4
Slag 6	1.2:1	42.29	30.19	4.80	4.80	2.88	9.6	1.44	4
Slag 7	1.2:1	41.41	29.63	4.80	4.80	2.88	9.6	2.88	4
Slag 8	1.21:1	37.15	29.05	8.87	3.28	3.45	3.67	2.67	0.38

Slag 1–Slag 7 refer to the simulated slags, Slag 8 refers to the industrial copper smelting slag. In addition to the above components in Table 1, Slag 8 also contains 3.86 wt.% PbO, 2.31 wt.% ZnO, 1.34 wt.% K_2O , 1.15 wt.% CuO, 0.64 wt.% SO_3 , and 0.81 wt.% Sb_2O_3

To evaluate the stability of arsenic in the actual slag, arsenic vitrification was also performed using industrial copper smelting slags obtained from a smelter in Shandong Province, China. In addition, industrial arsenic-containing solid generated by the same company, calcium arsenate, (22.5 wt.% As and 35.4 wt.% CaO) was selected as the raw material for vitrification and its corresponding XRD pattern is shown in Fig. S1(b) in Supporting Information. Similar to the simulated slags, arsenic was dispensed at 4 wt.%. The chemical composition of the industrial copper smelting slag (Slag 8) is also listed in Table 1. Notably, the industrial slag contains 0.38 wt.% As. Besides the metal oxides investigated, it also contains more basic oxides, such as PbO, ZnO and K_2O .

According to the intended composition of the sample, about 100 g of the mixture was stirred well in an agate mortar and transferred into a molybdenum crucible. Subsequently, the sample was heated to 1250 °C within a tube furnace under the protection of Ar at a flow rate of 0.4 L/min. The temperature was maintained for a duration of 1 h. Throughout the holding period, a delicate molybdenum rod was employed to stir the slag deeply, ensuring homogenization and stabilization of the sample. Upon completion of the holding period, the samples were rapidly quenched by repeatedly immersing a fine molybdenum rod into the molten pool and subsequently submerging it into water. Then, the samples were dried and crushed in preparation for subsequent experiments.

2.2 Characterization method

The composition of samples was measured by

inductively coupled plasma optical emission spectrometry (ICP-OES). The K₂Cr₂O₇ titration method was used to measure the contents of TFe and Fe²⁺. The crystal structure of the samples was analyzed using XRD. SEM was employed to examine the microscopic morphology of the quenched samples. FTIR and XPS were utilized for the characterization of the sample structure. The stability of the simulated slags was evaluated using TCLP and SPLP test, respectively. In the TCLP test, about 20 g of quenched samples were placed into a polyethylene bottle and acetate buffer solution with pH 4.93±0.05 was added at a liquid-solid ratio of 20:1 (mL/g). The samples were tumbled and shaken in a flip oscillator at (30±2) r/min for 18 h at room temperature. For the SPLP test, the leaching agent consisted of a mixture of sulfuric acid and nitric acid in a mass ratio of 6:4, with a pH value of 4.20±0.05. Other experimental parameters used for SPLP test are the same as those for the TCLP test. For the actual smelting slag, pH dependence experiment [23] was also adopted. The leaching agents with nine different pH values (2.0, 4.0, 5.5, 7.0, 9.0, 10.5, 11.0, 12.0 and 13.0) were prepared with dilute nitric acid and sodium hydroxide solution. The liquid/solid ratio was 10:1, and the leaching time was 48 h. The heating rate in DSC experiments was 10 °C/min, and the temperature range was 25–1250 °C with Ar atmosphere.

3 Results and discussion

3.1 Glass formation and analyzed compositions

The XRD patterns of the quenched slag samples with varying As and MgO contents are illustrated in Fig. 1(a). The absence of distinct

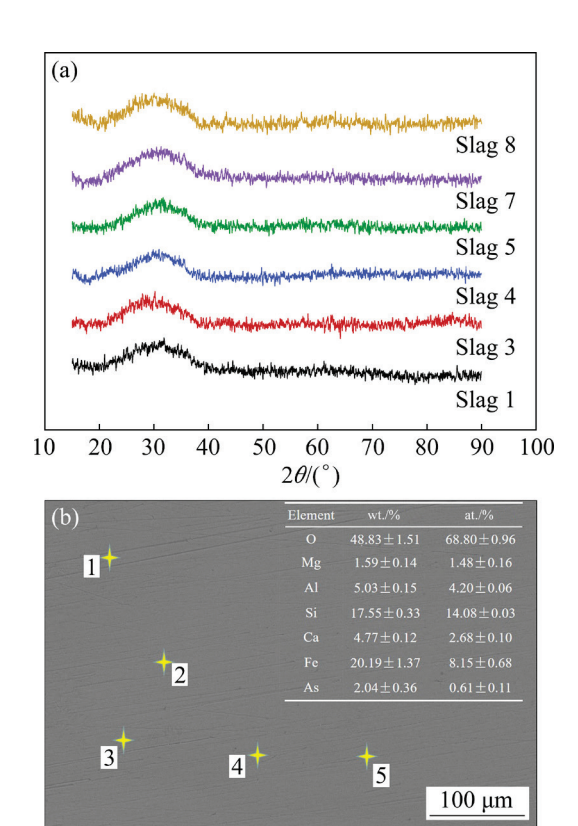


Fig. 1 XRD patterns of As-containing glasses with different As and MgO contents (a) and SEM image of typical specimen at 1.5 wt.% MgO (b)

crystal peaks in both the simulated slags and industrial slag confirms the amorphous, glassy structure of the samples. Moreover, Fig. 1(b) shows the microscopic morphology of a representative quenched slag sample along with the average results of EDS analysis. The surface of the sample is relatively smooth, without any evidence of crystalline phases, thus supporting the formation of glass. These XRD and SEM observations indicate that arsenic is effectively incorporated into

the iron-silicate slag at elevated temperatures, exhibiting good compatibility.

Table 2 gives the chemical composition of glasses after high-temperature melting. The As content in the samples decreases volatilization, while the Fe₂O₃ content increases, corresponding to a reduction in the content of FeO. This decrease in FeO can be attributed to the oxidation of Fe²⁺. Changes in the composition of the above substances in turn lead to variations in the chemical composition of other compounds. Moreover, the addition of MgO can slightly reduce the volatilization of arsenic and increase the As content in the glass. As can be seen from Table 2, the simulated iron-silicate slag can immobilize a minimum of 3.25 wt.% of arsenic. For the actual industrial slag, it contains a large amount of alkali metal oxides, which dissociate free oxygen at high temperatures, thereby compromising the silicate network structure. As a consequence, the slag demonstrates a diminished capacity for arsenic fixation. It should be noted that the use of molybdenum crucible inevitably results in a slight contamination with (0.5-1.0) wt.% MoO₃ and is therefore negligible.

3.2 FTIR spectra

Figure 2(a) illustrates the variations in the FTIR spectra of the slag with different As additions. It can be observed that the glass bodies exhibit similar spectral characteristics. In particular, the vibrational band width of [SiO₄]⁴⁻ tetrahedra, located at 1200–750 cm⁻¹ [27], becomes progressively narrower as the As content increases. This narrowing indicates a decrease in the distance between Si and O atoms and an increase in the polymerization of

Table 2 Experimentally determined chemical compositions of glass samples after high-temperature melting

Sample ID	Fe/SiO ₂ mass ratio	Content/wt.%							
		FeO	SiO_2	Fe_2O_3	B_2O_3	Al_2O_3	CaO	MgO	As
Slag 1	1.22:1	43.87	32.01	7.22	4.65	2.88	9.31	0	0
Slag 2	1.22:1	43.45	31.74	7.13	4.90	3.06	9.25	0	0.46
Slag 3	1.23:1	42.42	31.11	7.48	4.89	3.22	9.33	0	1.15
Slag 4	1.20:1	40.27	30.58	7.92	5.11	3.15	9.26	0	2.13
Slag 5	1.19:1	39.67	30.43	7.66	5.25	3.21	9.48	0	3.16
Slag 6	1.21:1	39.02	29.61	8.04	5.02	3.16	9.51	1.68	3.22
Slag 7	1.21:1	38.24	29.29	8.11	4.96	3.05	9.44	3.15	3.25
Slag 8	1.16:1	34.76	27.30	6.78	2.52	2.87	9.43	2.85	2.93

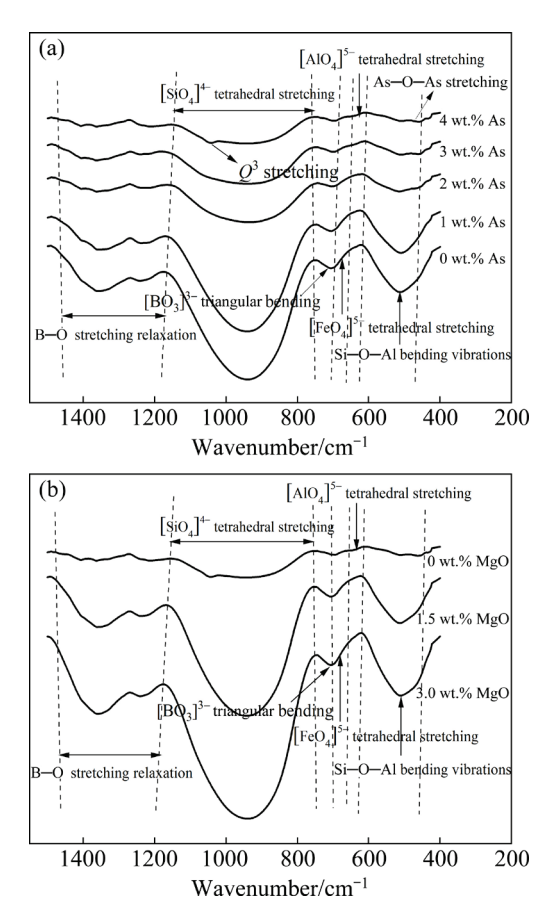


Fig. 2 FTIR spectra of As-containing glasses with different As (a) and MgO (b) contents

the silicate structure. Notably, at an As content of 4 wt.%, an absorption peak at 1050 cm⁻¹ becomes evident, which can be attributed to the vibrational band of Q^3 , corresponding to $[SiO_4]^{4-}$ tetrahedra with three bridging oxygen atoms [28]. This suggests that the addition of As results in a more complex silicate network structure. However, the depth of the $[SiO_4]^{4-}$ tetrahedral vibrational band and the bending vibrational band of Si—O—Al at a wavenumber of 500 cm⁻¹ [29] becomes shallower with increasing As content. This can be attributed to the decrease in SiO_2 content caused by the increased As content.

The wide band centered at around 1350 cm⁻¹ (including the single band at 1230, 1360 and 1430 cm⁻¹) is caused by the asymmetric tensile relaxation between the B—O bond of the triangular [BO₃] unit and the non-bridging oxygen (NBO) [30]. The intensity of the vibration band decreases with the As content, indicating a reduction in the number of [BO₃]³⁻ units and NBO. In addition, [BO₃]³⁻ also has a bending vibration band near 700 cm⁻¹ [31], and its vibration intensity gradually weakens with

the increase of As content. As a network modifier, it is known that [BO₃]³⁻ unit can provide NBO and depolymerize silicate structure. Thus, the addition of As reduces the number of NBO in the melt, and As participates in the construction of network structure. According to Ref. [32,33], the asymmetric stretching vibrational bands at about 690 and 620 cm⁻¹ are the vibrational peaks of [FeO₄]⁵⁻ and [AlO₄]⁵⁻ tetrahedra, respectively, which do not vary significantly. Furthermore, the stretching vibration of As -O - As appears at 470 cm⁻¹ [34], contributing to the broad and wide vibrational region in conjunction with the Si-O-Al band. Therefore, it is reasonable to speculate that As was involved in the formation of the glass lattice structure. A substantial amount of As enters the Si-O-Al-O framework as a constituent element, partially replacing Si and Al into the skeleton, making the polymerization of slag higher.

As we know, arsenic oxide (As₂O₃) acts as a strong network-forming component capable of absorbing free oxygen to form [AsO₄]³⁻ structures. From the ionic radius, ionic radii of Al3+, Si4+ and As $^{5+}$ are 0.57, 0.42 and 0.46 Å, respectively [35]. When examining bond lengths, the average lengths of the Al-O, Si-O, and As-O bonds are 1.75, 1.61, and 1.67 Å, respectively, all of which can form tetrahedral anions with oxygen, indicating that Si, As and O can form the same crystal structure. Therefore, it is considered that [AsO₄]³⁻, [SiO₄]⁴⁻ and [AlO₄]⁵⁻ can form an incomplete homogeneous phase. Specifically, [AsO₄]³⁻ can enter the Si-O-Al-O network structure and contribute to the formation of Si/Al-O-As chemical structures within the glass lattice.

Figure 2(b) shows the FTIR spectra of As-containing glass with different MgO contents. The center of gravity of the vibrational band located at 750-1200 cm⁻¹ gradually shifts towards lower wavenumbers, and the absorption band corresponding to the Q^3 structure becomes less prominent, indicating the depolymerization of the slag structure. In addition, the vibrational intensity of the [BO₃]³⁻ unit located at around 1350 and 700 cm⁻¹ gradually strengthens, indicating an increase in the NBO number and a decrease in the degree of polymerization of the slag. The vibrational peaks associated with the [FeO₄]⁵⁻ and [AlO₄]⁵⁻ units show minimal variation with the addition of MgO. However, the intensity of the vibrational band corresponding to Si—O—Al bonds is gradually strengthened probably because the addition of MgO brings a large amount of Mg²⁺, which is sufficient to satisfy the charge compensation required for the formation of the [AlO₄]⁵⁻ and [SiO₄]⁴⁻ cross-linked network structures.

3.3 XPS spectra

To further investigate the effect of As and MgO on slag structure, a series of XPS tests were performed on the As-containing glasses, and the results are shown in Fig. 3. The survey scan spectrum provides an overview of the elements present in the slag, including Mg, Fe, O, Ca, C, B, Si, Al, and As. The binding energy of the inner shell layer of atoms can be influenced by the chemical environment they are in. Therefore, the variation of the chemical shifts and intensities of the spectral peaks provide insight into the mechanism underlying the effects of As and MgO doping on the slag structure.

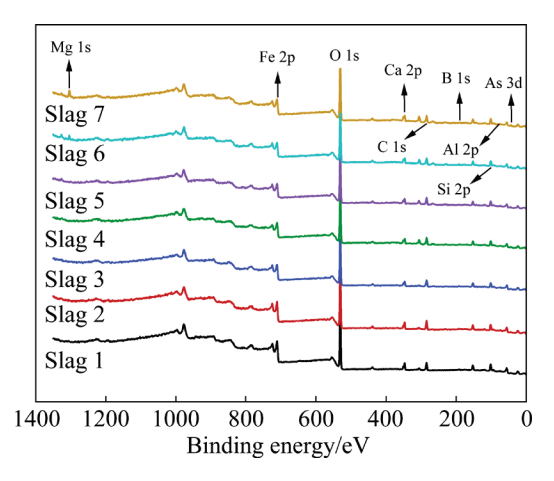


Fig. 3 Survey scan XPS spectra of As-containing glasses with different As and MgO contents

3.3.1 Si 2p spectra

Figure 4 shows the high-resolution scan spectra of Si atoms in As-containing glass with different As and MgO additions. It can be seen that the binding energy of Si atoms increases by a total of 0.42 eV as the As content increases from 0 to 4 wt.%. According to relevant literature [36], an increase in electron density on an atom results in electron shielding in its core layer, leading to a decrease in the effective positive charge and, consequently, a decrease in the binding energy.

Therefore, the observed increase in the binding energy of Si atoms suggests a reduction in the electron density on the Si nucleus. As mentioned in FTIR analysis, As can partially substitute Si and Al within the silicate framework to form the Si—O—As structure. Since the electronegativity of As (2.18) is larger than that of Si (1.98), the electron density on the O atom in the Si—O—As bond becomes more favorable for As. This preference for As causes a decrease in the average electron density on the Si atom. As a result, the binding energy of Si atoms increases.

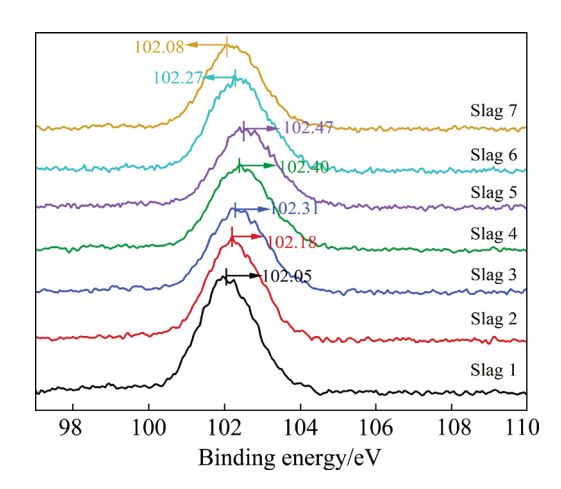


Fig. 4 High-resolution scan spectra of Si 2p of Ascontaining glasses with different As and MgO contents

Moreover, with the addition of MgO, the binding energy of Si atoms decreases, indicating an increase in the electron density on Si. To explain this change, the concept of Q^i was introduced [37]. Q^i represents different structural units in the silicate network, where i denotes the amount of bridging oxygen connected to Si atoms in each siliconoxygen tetrahedron. The addition of MgO introduces a large number of free oxygen ions (O²⁻), which depolymerize the silicate network structure. As a result, a considerable number of bridging oxygen structures are disrupted. This disruption is reflected in a decrease in the value of i, representing a decrease in the number of bridging oxygen atoms combined with Si atoms. Therefore, the average electron density on the central Si atom increases, which reduces the binding energy.

Since the number of bridging and non-bridging oxygen atoms bound by the tetrahedrally coordinated Si atoms in different Q^i species varies, each Q^i unit may produce an independent vibration. It has been reported that the binding energies of

Si $2p_{3/2}$ for Q^0 , Q^2 , and Q^4 species are 101.7, 102.7, and 103.85 eV, respectively [38,39]. As mentioned earlier, the average electron density on the silicon-oxygen tetrahedron will increase with more non-bridging oxygen atoms. Consequently, it can be inferred that the binding energy of Si 2p will decrease sequentially from Q^4 to Q^0 . In addition, it has been shown that each Q^i species in the silicate network structure has approximately the same FWHM [40]. Based on this, the vibrational peaks of Si 2p were fitted to explore the transition of Q^i species with the addition of As and MgO. Figure 5 shows typical deconvolution diagrams of Si 2p for different As and MgO contents, and the rest are shown in Fig. S2 in Supporting Information.

As can be seen in Fig. 5, Q^0 (29.99%), Q^1 (48.63%) and Q^2 (21.38%) structural units are present in the undoped sample. With the initial addition of As, the Q^3 structural unit (7.90%) starts to appear. The subsequent increase in the As content leads to a continuous increase in the molar fraction of the Q^3 unit, while the relative contents of the Q^0

and Q^1 units decrease. This further indicates that As enters into the silicate network structure as a constituent element, resulting in an increase in the number of bridging oxygen in the slag. In contrast, the doping of MgO leads to an increase in the molar fraction of Q^0 and Q^1 , while the relative content of Q^3 decreases. This implies that MgO acts as a network modifier, providing non-bridging oxygen species that contribute to the depolymerization of the slag structure.

3.3.2 O 1s spectra

The variation of the O 1s binding energy with As and MgO contents is given in Fig. 6. With increasing As content, the binding energy of O atoms increases, with an increase of about 0.34 eV over the range of compositions studied. For the addition of MgO, the change of O 1s binding energy is just the opposite. This trend is easily understood because As enters the silicate network structure in the form of [AsO₄]³⁻, forming a more aggregated complex anion population (Si—O—As). Because As is more electronegative than Si, the

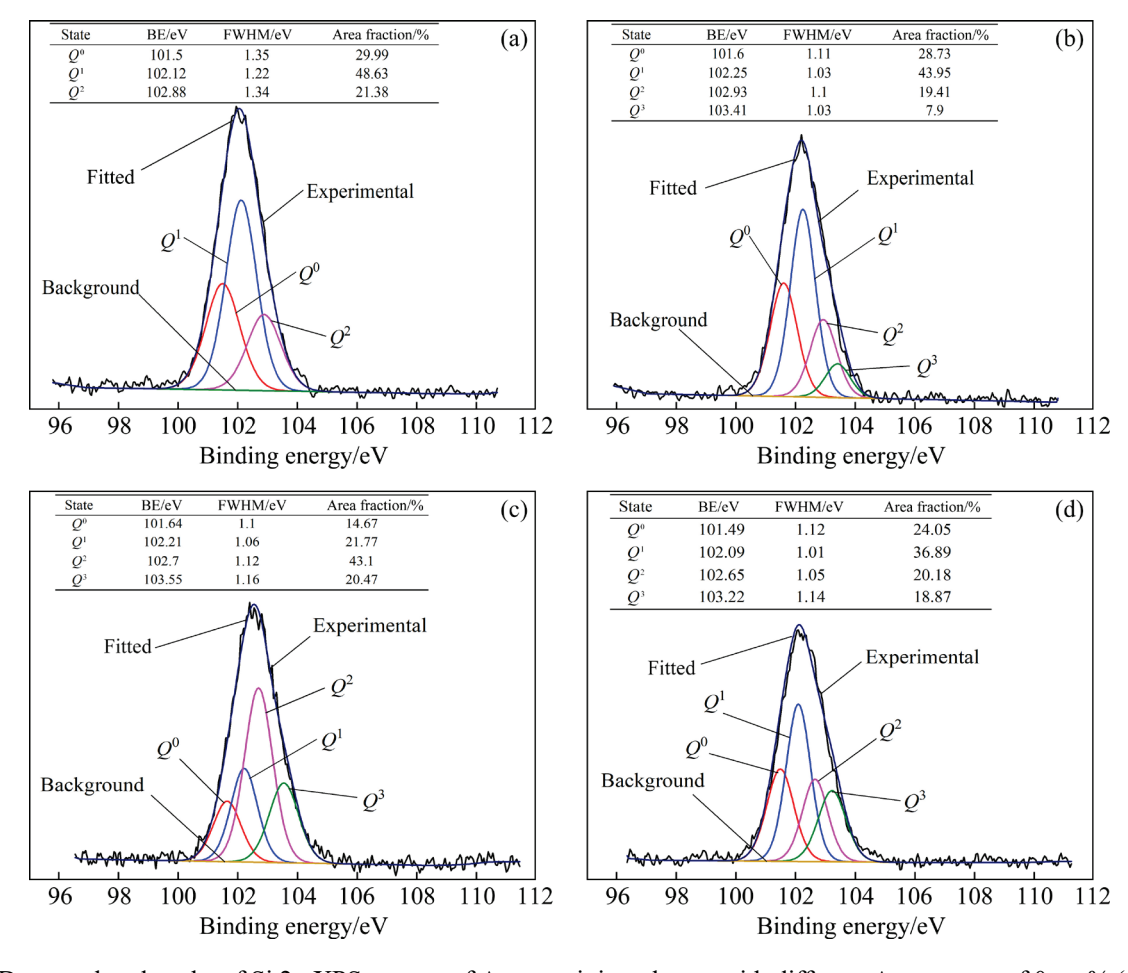


Fig. 5 Deconvoluted peaks of Si 2p XPS spectra of As-containing glasses with different As contents of 0 wt.% (a), 1 wt.% (b), and 4 wt.% (c), and MgO content of 3 wt.% (d)

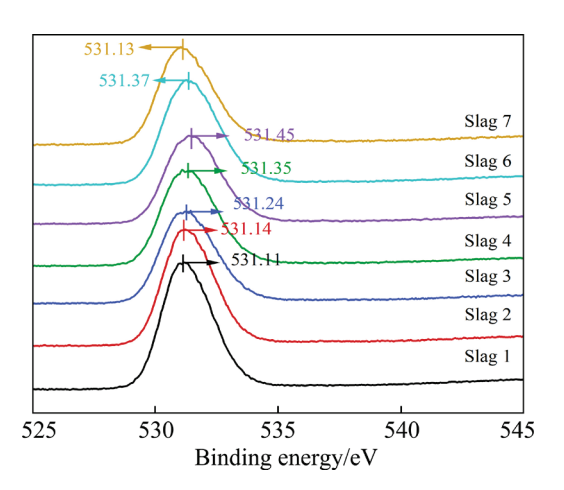


Fig. 6 Changes in binding energy of O 1s with different As and MgO contents

electron density on O atoms in Si—O—As is lower than that in Si—O—Si, which in turn reduces the measured binding energy. In addition, as the electron density on Si atoms decreases with the addition of As, the electron density on O atoms to which different types of Si atoms are attached will

also decrease, further contributing to the rise in binding energy. For MgO, the decrease in the binding energy of O atoms indicates an increase in the electron density, which is due to the increase in the number of the NBO in the slag. Mg can effectively release its outer electrons to the non-bridging oxygen, thus making the binding energy decrease.

The O 1s spectrum contains the contribution of all oxygen atoms in the As-containing glass. To clarify the evolution of different types of O atoms with the addition of As and MgO, the O 1s spectrum was deconvoluted and the results are shown in Fig. 7 and Fig. S3 in Supporting Information, and the corresponding fitted parameters are shown in Table 3 and Table S1 in Supporting Information. In the absence of As doping, bridging oxygen (Si—O—Si) and non-bridging oxygen (Si—O—Me) are present in the slag. The electron binding energy of O 1s in Si—O—Si is higher than that in Si—O—Me because the metal atoms can transfer the outer electrons to the O atoms. In our study, no peak splitting

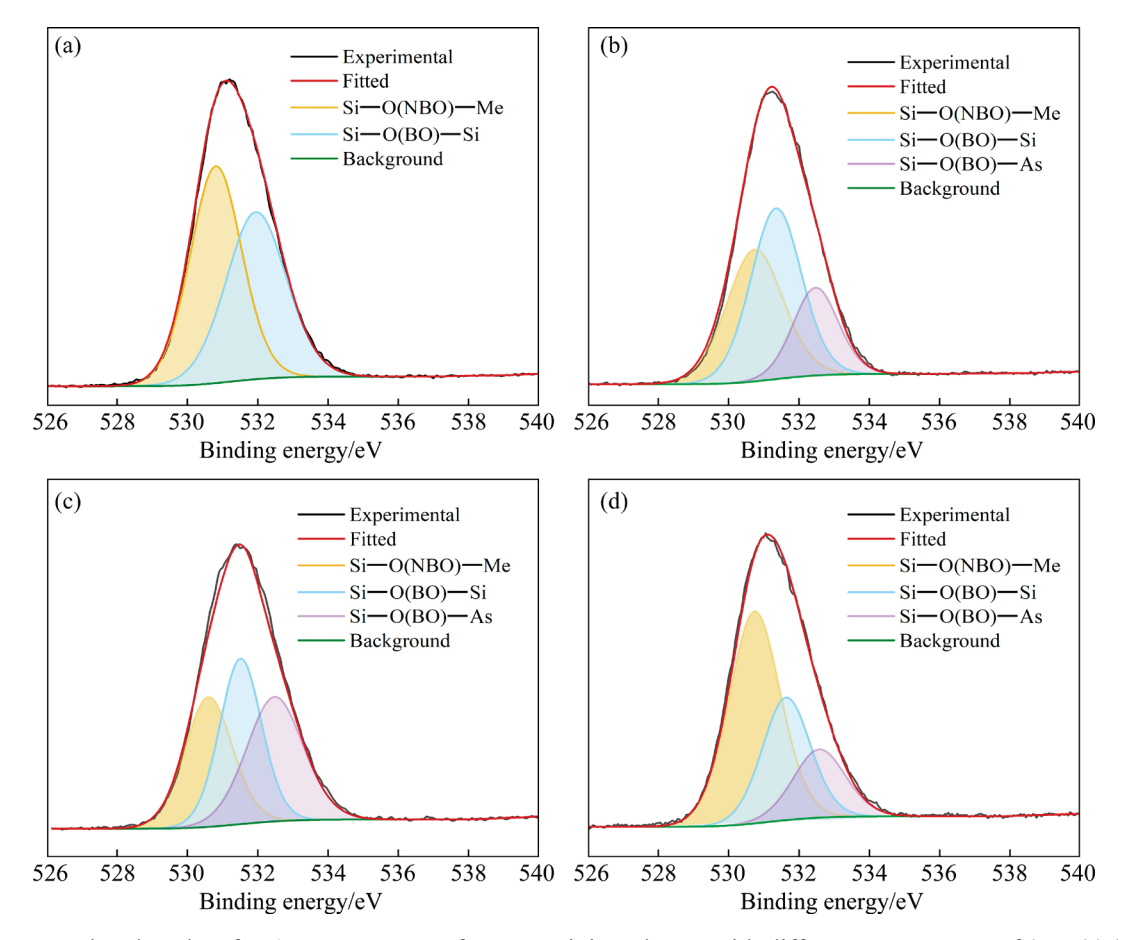


Fig. 7 Deconvoluted peaks of O 1s XPS spectra of As-containing glasses with different As contents of 0 wt.% (a), 1 wt.% (b), and 4 wt.% (c), and MgO content of 3 wt.% (d)

Table 3 Peak information of fitted peaks of O 1s spectra in Slags 1, 2, 5 and 7

Slag No.	State	BE/eV	FWHM/eV	Area fraction/%	
1	Si—O—Me	530.81	1.72	52.60	
	Si—O—Si	531.95	2.02	47.40	
2	Si—O—Me	530.74	1.90	37.21	
	Si—O—Si	531.35	1.69	42.96	
	Si-O-As	532.48	1.52	19.83	
5	Si—O—Me	530.60	1.61	30.83	
	Si—O—Si	531.51	1.40	34.34	
	Si-O-As	532.48	1.90	34.93	
7	Si—O—Me	530.74	1.73	53.69	
	Si—O—Si	531.64	1.61	28.81	
	Si-O-As	532.58	1.75	17.51	

was performed for free oxygen. Since the contribution of free oxygen is very close to that of non-bridging oxygen, the O²⁻ signal cannot be resolved in the XPS spectrum [38,40]. At As addition of 1 wt.%, Si-O-As starts to appear in the slag and its relative content increases gradually with increasing As content. It can be seen from Table 3 and Table S1 that the relative content of Si—O—Si decreases with the addition of As, which is due to the conversion of part of Si-O-Si to Si—O—As. As mentioned earlier, the NBO number in the slag decreases with the addition of As, and therefore the relative content of Si - O - Me decreases accordingly. In addition, the addition of MgO promotes the depolymerization of the bridging oxygen structure and increases the NBO number. This corresponds to a decrease in the relative contents of Si-O-As and Si-O-Si structures and an increase in the relative content of Si—O—Me, respectively.

3.3.3 As 3d and B 1s spectra

Figure 8(a) shows the variations of binding energy of As 3d with As and MgO contents in the sample. It can be seen that with the continuous addition of As, the intensity of the As 3d peak is gradually strengthened. Additionally, the binding energy of As 3d shows a decreasing tendency, which indicates the increase of the electron density on the nucleus of As atoms. The addition of As transforms part of the Si—O—Si structure into the Si—O—As structure. Based on the electronegativity difference between As and Si atoms, it is easier for As to gain electrons in the

Si—O—As bond relative to Si. As a result, the binding energy of As atoms decreases. Similarly, with the addition of MgO, the binding energy of As 3d moves to a lower position due to the free oxygen brought by MgO that can break the Si—O—As structure and form Mg/Ca/Fe—O—As chemical bonds. These metal atoms transfer their electrons to As, leading to an increase in the electron density on the nucleus of As and a consequent decrease in the binding energy.

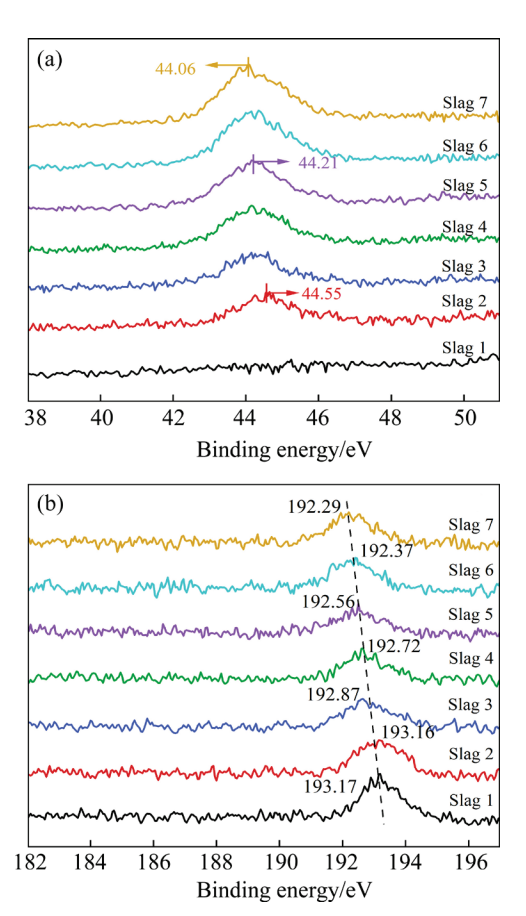


Fig. 8 Changes in binding energy of As 3d (a) and B 1s (b) spectra with different As and MgO contents

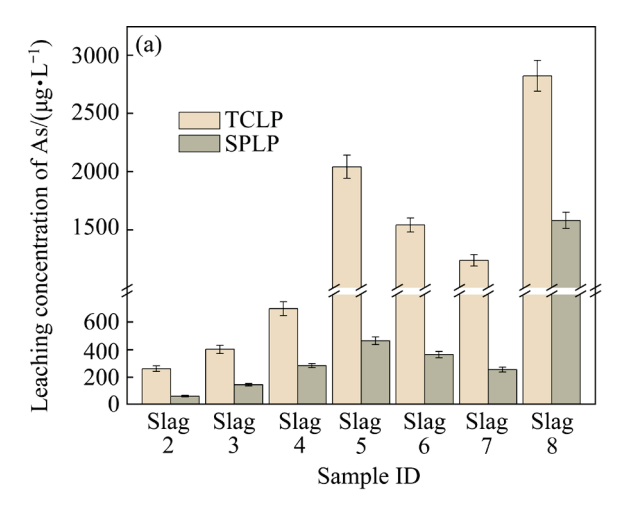
The variations of B 1s binding energy with As and MgO contents are shown in Fig. 8(b). It can be seen that the binding energy of B 1s decreases from 193.17 to 192.56 eV with the increase of As content from 0 to 4 wt.%. This decrease in binding energy is relatively significant and indicates that As has a pronounced effect on the borate structure. According to the relevant literature [41], the binding energy of the [BO₃]³⁻ structural unit is about 193.0 eV, while the binding energy of borates containing both [BO₃]³⁻ and [BO₄]⁵⁻ structural units is about 192.4 eV. With the addition of As, the B 1s binding energy shifts towards lower chemical shifts.

This indicates a decrease in the [BO₃]³⁻ structure and an increase in the [BO₄]⁵⁻ structure in the slag, which is consistent with the conclusion obtained from FTIR spectra. Moreover, the binding energy of B 1s decreases with the addition of MgO. A reasonable explanation is that the electronegativity of B is relatively large (2.04), and MgO depolymerizes the borosilicate structure, causing the B — O — Si bond to gradually become a B—O—Me bond. This transformation increases the electron density around the B atom, resulting in a decrease in the measured binding energy.

3.4 Stability of As-containing slag

3.4.1 Leaching toxicities

To evaluate the chemical stability of As in vitreous, TCLP and SPLP tests were performed and the results are shown in Fig. 9(a). For the simulated copper slags (Slag 2-Slag 7), the TCLP and SPLP test results showed good agreement, i.e., the concentration of As in the leachate gradually increased with the increase of As content. The addition of MgO effectively reduced the leaching concentration of As. All these values were below the standard threshold (5 mg/L) set by USEPA. However, for the actual copper smelting slag (Slag 8), the leaching concentration of As was higher than the results in the simulated copper slags. This disparity can be attributed to the presence of other components in the industrial smelting slags, such as K₂O, PbO, and ZnO, and these metal oxides can disrupt the network structure of silicates at high temperatures, making the slag less stable. It is worth pointing out that the leaching concentrations of As in SPLP were lower than those in TCLP tests, both for simulated and actual copper smelting slags. In our experiment, for TCLP test acetic acidsodium acetate buffer solution was used, which can stabilize the pH value of the solution within a specific range, and As can be easily leached under this condition. Table S2 in Supporting Information lists the final pH values of leachate in different experimental groups. It can be seen that the pH values after leaching in TCLP experiment remained stable between 4.9 and 5.4 with minimal changes. In contrast, for SPLP test, the final pH of the leachate was around 7.0. Although the initial lower pH in the SPLP test facilitates the leaching of As, the solution does not have a buffering capacity and therefore the leaching of As is low.



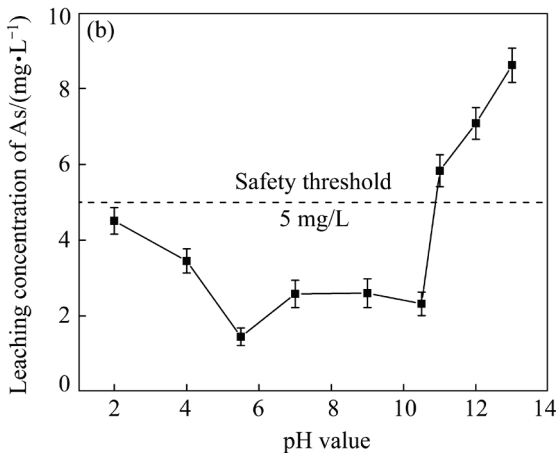


Fig. 9 Leaching toxicity test results of As from glasses using TCLP and SPLP tests (a) and pH dependency results for industrial slag (b)

The stability of As in the actual smelting slag was further investigated by examining its leaching characteristics at different pH values, following the study conducted by MAHANDRA et al [23]. From Fig. 9(b), it can be seen that the leaching curve of As shows a "V" shaped pattern, with the least release under weak acid to weak base conditions. The leaching concentration of As changed rapidly with pH under more acidic conditions and strong alkaline conditions. In particular, the leaching concentration of As exceeded the safety limit of 5 mg/L at an initial pH > 11. Similar leaching behavior trends were observed in the assessment of arsenic stability in the glass sample produced using As-containing flue dust in GlassLockTM process, and this variation can be attributed to the amphoteric nature of arsenic [21-23]. Table S3 in Supporting Information provides the final pH of the leachate. Under alkaline conditions, a slight decrease in pH value occurs, which can be

attributed to the dissociation of protons in the sample, allowing the presence of $H_2AsO_4^-$, $HAsO_4^{2-}$ and AsO_4^{3-} species in the solution [42].

The fundamental purpose of vitrification of arsenic is to judge whether arsenate enters the silicate network structure through chemical reaction. There is no doubt that if arsenic exists in the melt in the form of calcium arsenate, the solubility of As in the acid-leaching solution is bound to be very high. For this reason, two different types of calcium arsenates used in the experiment were tested by TCLP. The results showed that the As concentration of self-made calcium arsenate and industrial calcium arsenate reached 6.85 mg/L and 1.07 g/L, respectively, which both exceeded the safety limit. In our study, the leaching concentration of As remained low in all cases, meeting the requirements of industrial emissions. Therefore, it can be concluded that As replaces part of Si or Al into the Si-O-Al-O skeleton, forming a more complex anion group and enhancing the chemical stability of the glass. Although the addition of MgO can depolymerize the silicate network structure, it can also form a more stable structure in the melt, namely As—O—Me [43,44]. This formation of a stable structure contributes to the reduction in the leaching concentration of As, as confirmed by the XPS analysis described earlier.

3.4.2 DSC curves

In order to analyze the effect of As and MgO addition on the thermal stability of glass, DSC analysis of slag was performed and the results are shown in Fig. 10. The glass transition temperature (T_g) and the onset of crystallization temperature (T_c) are widely recognized parameters for evaluating the thermal stability characteristics of glass, and these two temperatures can be deduced from the DSC curves using the tangent method [45]. According to the relevant literature [18,46], the larger the difference between the two temperatures $(\Delta T (= T_c - T_g))$, the better the thermal stability of the glass, and the greater the resistance to crystallization. In our study, the disparity in T_g among the glasses with varying As and MgO contents was not substantial, predominantly falling within the range of (520 ± 3) °C. However, the discrepancy in T_c exhibited a more noticeable pattern, showing an upward trend. As the As content increased from 0 to 4 wt.%, the ΔT value rose from 119 to 132 °C, indicating that As reinforced the silicate network structure. With the doping of 3 wt.% of MgO, the ΔT value further increased to 142 °C, indicating that the addition of MgO can enhance the thermal stability of As-containing slag and mitigate the propensity for glass crystallization.

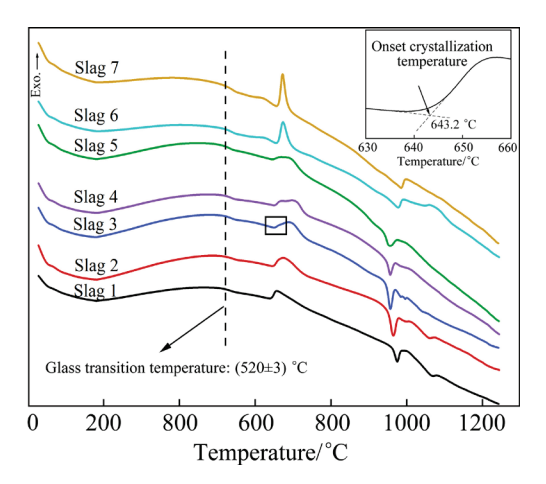


Fig. 10 DSC curves of As-containing glasses at different As and MgO contents

4 Conclusions

- (1) Arsenic exhibited good compatibility with copper smelting slag, both for simulated and industrial slag. The iron-silicate type slag could successfully vitrify about 3 wt.% of As.
- (2) The addition of As makes the molar fraction of the Q^3 unit increase, while the relative contents of the Q^0 and Q^1 units decrease. In addition, As can partially replace Si into the silicate skeleton to form the Si—O—As structure.
- (3) The introduction of MgO caused the depolymerization of the bridging oxygen structure and an increase in the NBO number, which corresponds to the decrease of the relative content of Si—O—As and Si—O—Si structures and the increase of the Si—O—Me, respectively.
- (4) The leaching toxicity of As exhibited a gradual increase with the addition of As. Adding MgO demonstrated a mitigating effect on the leaching toxicity of As. As exhibited amphoteric behavior in pH-dependent experiments.
- (5) DSC analysis showed that As can strengthen the silicate network structure. The incorporation of MgO can improve the thermal stability of As-containing slag.

CRediT authorship contribution statement

Zhe-nan JIN: Resources, Project administration,

Conceptualization, Investigation; **Bao-ren WANG:** Investigation, Formal analysis, Writing – Original draft preparation, Writing – Reviewing and editing; **Hong-ying YANG:** Resources, Supervision; **Qian-fei ZHAO:** Investigation, Formal analysis, Supervision; **Yan FU:** Resources, Visualization, Supervision.

Declaration of competing interest

The authors declare that they have no known competing financial interests or personal relationships that could have appeared to influence the work reported in this paper.

Acknowledgments

This work was supported by the National Key R&D Program of China (No. 2018YFC1902004).

Supporting Information

Supporting Information in this paper can be found at: http://tnmsc.csu.edu.cn/download/22-p2020-2022-1289-Supporting Information.pdf.

References

- [1] DIMITRIJEVIĆ M, KOSTOV A, TASIĆ V, MILOSEVIĆ N. Influence of pyrometallurgical copper production on the environment [J]. Journal of Hazardous Materials, 2009, 164(2/3): 892–899.
- [2] MOSKALYK R R, ALFANTAZI A M. Review of copper pyrometallurgical practice: Today and tomorrow [J]. Minerals Engineering, 2003, 16(10): 893–919.
- [3] ZHANG Hui-bin, WANG Ya-nan, ZHU Yin-bin, REN Pen, HU Bin, XU Sheng-hang, CAO Hua-zhen, ZHOU Jun, ZHENG Guo-qu. Determination of occurrence and leaching toxicity of arsenic in copper flash smelting slags [J]. Transactions of Nonferrous Metals Society of China, 2023, 33(1): 293-303.
- [4] ZHANG Hui-bin, WANG Ya-nan, HE Yu-zheng, XU Sheng-hang, HU Bin, CAO Hua-zhen, ZHOU Jun, ZHENG Guo-qu. Efficient and safe disposition of arsenic by incorporation in smelting slag through copper flash smelting process [J]. Minerals Engineering, 2021, 160: 106661.
- [5] YANG Wei-chun, TIAN Shun-qi, WU Jian-xun, CHAI Li-yuan, LIAO Qi. Distribution and behavior of arsenic during the reducing-matting smelting process [J]. JOM, 2017, 69(6): 1077–1083.
- [6] SHIBAYAMA A, TAKASAKI Y, WILLIAM T, YAMATODANI A, HIGUCHI Y, SUNAGAWA S, ONO E. Treatment of smelting residue for arsenic removal and recovery of copper using pyro-hydrometallurgical process [J]. Journal of Hazardous Materials, 2010, 181(1/2/3): 1016–1023.
- [7] CUI Jie, DU Ya-guang, XIAO Hong-xia, YI Qiu-shi, DU Dong-yun. A new process of continuous three-stage co-precipitation of arsenic with ferrous iron and lime [J]. Hydrometallurgy, 2014, 146: 169–174.

- [8] CAETANO M L, CIMINELLI V S T, ROCHA S D F, SPITALE M C, CALDEIRA C L. Batch and continuous precipitation of scorodite from dilute industrial solutions [J]. Hydrometallurgy, 2009, 95(1/2): 44–52.
- [9] MOON D H, DERMATAS D, MENOUNOU N. Arsenic immobilization by calcium-arsenic precipitates in lime treated soils [J]. Science of the Total Environment, 2004, 330(1/2/3): 171-185.
- [10] NAZARI A M, RADZINSKI R, GHAHREMAN A. Review of arsenic metallurgy: Treatment of arsenical minerals and the immobilization of arsenic [J]. Hydrometallurgy, 2017, 174: 258–281.
- [11] ADELMAN J G, ELOUATIK S, DEMOPOULOS G P. Investigation of sodium silicate-derived gels as encapsulants for hazardous materials – The case of scorodite [J]. Journal of Hazardous Materials, 2015, 292: 108–117.
- [12] LIU Shou-qing, LUO Zhong-qiu, HE Sen, ZHOU Xin-tao, JIA Qing-ming. Solidification/stabilization of calcium arsenate waste with blast furnace slag and fly ash geopolymer materials [J]. Chemical industry and engineering progress, 2017, 36(7): 2660–2666. (in Chinese)
- [13] TIAN Jia, SUN Wei, ZHANG Xing-fei, HAN Hai-sheng, YU Zhi-yuan, YUE Tong, WANG Li, YANG Yue, TANG Hong-hu, LI Er-ping. Comprehensive utilization and safe disposal of hazardous arsenic—alkali slag by the combination of beneficiation and metallurgy [J]. Journal of Cleaner Production, 2021, 295: 126381.
- [14] LIU J, CHI R, ZENG Z, LIANG J, XU Z. Selective arsenic-fixing roast of refractory gold concentrate [J]. Metallurgical and Materials Transactions B, 2000, 31(6): 1163–1168.
- [15] XU Bin, MA Yong-peng, GAO Wei, YANG Jun-kui, YANG Yong-bin, LI Qian, JIANG Tao. A review of the comprehensive recovery of valuable elements from copper smelting open-circuit dust and arsenic treatment [J]. JOM, 2020, 72(11): 3860–3875.
- [16] LEE T, OH J I, YI H, TSANG Y F, KWON E E. Fabrication of carbon-slag composite via a pyrolytic platform and its environmental application for arsenic removal as a case study [J]. Chemical Engineering Journal, 2019, 361: 1630–1639.
- [17] ZHAO Zong-wen, CHAI Li-yuan, PENG Bing, LIANG Yan-jie, HE Ying-he, YAN Zi-hao. Arsenic vitrification by copper slag based glass: Mechanism and stability studies [J]. Journal of Non-Crystalline Solids, 2017, 466/467: 21–28.
- [18] SHI Mei-qing, LIANG Yan-jie, CHAI Li-yuan, MIN Xiao-bo, ZHAO Zong-wen, YANG Shu. Raman and FTIR spectra of modified iron phosphate glasses containing arsenic [J]. Journal of Molecular Structure, 2015, 1081: 389–394.
- [19] WANG Da-wei, ZHAO Zong-wen, LIN Zhang, LIANG Yan-jie, KANG Li, PENG Bing. Interaction mechanism between arsenate and fayalite-type copper slag at high temperatures [J]. Transactions of Nonferrous Metals Society of China, 2022, 32(2): 709–720.
- [20] REDDY R G, FONT J M. Arsenate capacities of copper smelting slags [J]. Metallurgical and Materials Transactions B, 2003, 34(5): 565–571.
- [21] Dundee Sustainable Technologies (DST). GlassLock, ProcessTM [EB/OL]. [2022–01–12]. http://dundeetechnologies.

- com/glasslock-process.
- [22] MAHANDRA H, AZIZITORGHABEH A, GHAHREMAN A. Comparative study for flue dust stabilization in cement and glass materials: A stability assessment of arsenic [J]. Minerals, 2022, 12(8): 939.
- [23] MAHANDRA H, WU C Q, GHAHREMAN A. Leaching characteristics and stability assessment of sequestered arsenic in flue dust based glass [J]. Chemosphere, 2021, 276: 130173.
- [24] ZHAO Zong-wen, SONG Yu-xia, MIN Xiao-bo, LIANG Yan-jie, CHAI Li-yuan, SHI Mei-qing. XPS and FTIR studies of sodium arsenate vitrification by cullet [J]. Journal of Non-Crystalline Solids, 2016, 452: 238–244.
- [25] BHARGAVA A, SNYDER R L, CONDRATE S R A. The Raman and infrared spectra of the glasses in the system BaO-TiO₂-B₂O₃ [J]. Materials Research Bulletin, 1987, 22(12): 1603–1611.
- [26] WANG Bao-ren, YANG Hong-ying, JIN Zhe-nan, ZHAO Qian-fei, FU Yan. Effect of Fe/SiO₂ ratio and cooling regime on As stability in copper smelting slag [J]. Journal of Non-Crystalline Solids, 2023, 606: 122190.
- [27] PARK H, PARK J Y, KIM G H, SOHN I. Effect of TiO₂ on the viscosity and slag structure in blast furnace type slags [J]. Steel Research International, 2012, 83(2): 150–156.
- [28] JIN Zhe-nan, WANG Bao-ren, LIU Zhi-jian, YANG Hong-ying, ZOU Ming-jun, FU Yan. Effects of Fe/SiO₂ ratio and MgO content on the viscous behaviors of the SiO₂–FeO–MgO–12wt.%Fe₂O₃–8wt.%CaO–3wt.%Al₂O₃ slag system [J]. Metallurgical and Materials Transactions B, 2022, 53(2): 902–915.
- [29] PARK H, PARK S S, SOHN I. The viscous behavior of FeOt–Al₂O₃–SiO₂ copper smelting slags [J]. Metallurgical and Materials Transactions B, 2011, 42(4): 692–699.
- [30] MANSOUR E. Semi-quantitative analysis for FTIR spectra of Al₂O₃–PbO–B₂O₃–SiO₂ glasses [J]. Journal of Non-Crystalline Solids, 2012, 358(3): 454–460.
- [31] HUANG San-xi, LI Sheng, WU Feng-nian, YUE Yun-long. Effect of B₂O₃ on structure and properties of CaO-MgO-B₂O₃-Al₂O₃-SiO₂ glasses [J]. Journal of Inorganic and Organometallic Polymers and Materials, 2015, 25(4): 816–822.
- [32] WANG Zhan-jun, SUN Yong-qi, SRIDHAR S, ZHANG Mei, GUO Min, ZHANG Zuo-tai. Selective crystallization behavior of CaO-SiO₂-Al₂O₃-MgO-FetO-P₂O₅ steelmaking slags modified through P₂O₅ and Al₂O₃ [J]. Metallurgical and Materials Transactions B, 2015, 46(5): 2246-2254.
- [33] LÜ Jian-fang, JIN Zhe-nan, YANG Hong-ying, TONG Lin-lin, CHEN Guo-bao, XIAO Fa-xin. Effect of the CaO/SiO₂ mass ratio and FeO content on the viscosity of CaO-SiO₂-"FeO"-12wt.%ZnO-3wt.%Al₂O₃ slags [J]. International Journal of Minerals, Metallurgy, and Materials, 2017, 24(7): 756–767.
- [34] GILLIAM S J, MERROW C N, KIRKBY S J, JENSEN J O, ZEROKA D, BANERJEE A. Raman spectroscopy of arsenolite: Crystalline cubic As₄O₆ [J]. Journal of Solid State

- Chemistry, 2003, 173(1): 54-58.
- [35] ZHAO Zong-wen, WANG Zhong-bin, XU Wen-bin, QIN Wei-ning, LEI Jie, DONG Zhun-qin, LIANG Yan-jie. Arsenic removal from copper slag matrix by high temperature sulfide-reduction-volatilization [J]. Journal of Hazardous Materials, 2021, 415: 125642.
- [36] WANG P W, ZHANG L P. Structural role of lead in lead silicate glasses derived from XPS spectra [J]. Journal of Non-Crystalline Solids, 1996, 194(1): 129–134.
- [37] WANG Bao-ren, YANG Hong-ying, JIN Zhe-nan, LIU Zhi-jian, ZOU Ming-jun. Effect of Fe/SiO₂ ratio and Fe₂O₃ on the viscosity and slag structure of copper-smelting slags [J]. Metals, 2022, 12(1): 24.
- [38] SAWYER R, NESBITT H W, SECCO R A. High resolution X-ray photoelectron spectroscopy (XPS) study of K₂O-SiO₂ glasses: Evidence for three types of O and at least two types of Si [J]. Journal of Non-Crystalline Solids, 2012, 358(2): 290–302.
- [39] ZAKAZNOVA-HERZOG V P, NESBITT H W, BANCROFT G M, TSE J S, GAO X, SKINNER W. High-resolution valence-band XPS spectra of the nonconductors quartz and olivine [J]. Physical Review B, 2005, 72(20): 205111–205113.
- [40] NESBITT H W, BANCROFT G M, HENDERSON G S, HO R, DALBY K N, HUANG Y, YAN Z. Bridging, non-bridging and free (O²⁻) oxygen in Na₂O-SiO₂ glasses: An X-ray Photoelectron Spectroscopic (XPS) and Nuclear Magnetic Resonance (NMR) study [J]. Journal of Non-Crystalline Solids, 2011, 357(1): 170-180.
- [41] LUO Wei, BAO Zhen-hong, JIANG Wei-hui, LIU Jian-min, FENG Guo, XU Yan-qiao, TANG Hui-dong, WANG Tao. Effect of B₂O₃ on the crystallization, structure and properties of MgO–Al₂O₃–SiO₂ glass-ceramics [J]. Ceramics International, 2019, 45(18): 24750–24756.
- [42] WU Cheng-qian, MAHANDRA H, GHAHREMAN A. Novel continuous column process for As(III) oxidation from concentrated acidic solutions with activated carbon catalysis [J]. Industrial & Engineering Chemistry Research, 2020, 59(21): 9882–9889.
- [43] CHAI Li-yuan, ZHAO Zong-wen, LIANG Yan-jie, MIN Xiao-bo, SHI Mei-qing, ZHOU Bo-sheng. Effects of CaO addition on structure and arsenic immobilization in sodium—iron—boron—phosphorous glass [J]. Nonferrous Metals Science and Engineering, 2015, 6: 1–7. (in Chinese)
- [44] QIAN Bin, LIANG Xiao-feng, WANG Cui-ling, YANG Shi-yuan. Structure and properties of calcium iron phosphate glasses [J]. Journal of Nuclear Materials, 2013, 443(1/2/3): 140–144.
- [45] JUNG S S, SOHN I. Crystallization control for remediation of an FetO-rich CaO-SiO₂-Al₂O₃-MgO EAF waste slag [J]. Environmental Science & Technology, 2014, 48(3): 1886–1892.
- [46] JHA K, JAYASIMHADRI M. Spectroscopic investigation on thermally stable Dy³⁺ doped zinc phosphate glasses for white light emitting diodes [J]. Journal of Alloys and Compounds, 2016, 688: 833–840.

As 和 MgO 的加入对铜冶炼渣中砷玻璃化的影响

金哲男 1,2, 王保仁 1,2, 杨洪英 1,2, 赵前飞 1,2, 符 岩 1,2

- 1. 东北大学 多金属矿生态冶金教育部重点实验室, 沈阳 110819;
 - 2. 东北大学 冶金学院, 沈阳 110819

摘 要: 研究 FeO— SiO_2 — Fe_2O_3 — B_2O_3 —CaO— Al_2O_3 —(MgO)体系铜冶炼渣中砷(As)的玻璃化。通过 XRD、SEM、FTIR 和 XPS 分析手段系统地研究 As 玻璃化机制。结果表明,As 与铁硅酸盐炉渣表现出良好的相容性。FTIR 和 XPS 分析结果表明,As 可以部分替代硅形成 Si—O—As 结构,从而提高熔体的聚合度。 $[BO_3]^3$ —结构单元随着 As 含量的增加而趋于减少,而加入 MgO 后则观察到相反的行为。此外,MgO 增加了熔体的非桥氧数量(NBO)。TCLP、SPLP 和 pH 依赖性测试结果表明,As 的浸出毒性随着 As 含量的增加而增加,但随着 MgO 的加入而降低。DSC 分析结果表明,As 和 MgO 的加入均可以改善含 As 玻璃的热稳定性。

关键词:玻璃化;砷;氧化镁;铜冶炼渣;炉渣结构

(Edited by Wei-ping CHEN)